RSC Advances

ROYAL SOCIETY OF CHEMISTRY

www.rsc.org/advances

Journal Name

ARTICLE

Nb_2O_5/Graphene nanocomposites for Electrochemical Energy Storage

Received 00th January 20xx,
Accepted 00th January 20xx

DOI: 10.1039/x0xx00000x

www.rsc.org/

Paulraj Arunkumar,[a,b] Ajithan G. Ashish,[a] Binson Babu,[a] Som Sarang,[a] Abhin Suresh,[a] Chithra H. Sharma,[a] Madhu Thalakulam[a] and Manikoth M. Shaijumon [a]*

Development of electrode materials for energy storage, with high energy and power densities along with good cyclic stability, still remains a big challenge. Here we report synthesis of Nb_2O_5/graphene nanocomposites through simple hydrothermal method, with Nb_2O_5 nanoparticles anchored on reduced graphene oxide (RGO) sheets. The fabricated Nb_2O_5/graphene electrodes exhibited excellent electrochemical performance when studied as anodes for Lithium-ion battery, with superior reversible capacity and high power capability (192 $mAhg^{-1}$ under 0.1C rate over 50 cycles). Signature curve' studies showed high power capability of Nb_2O_5/graphene electrode with ~80% of the total capacity retained at 16C rate compared to ~30% retention for pristine Nb_2O_5 nanoparticles. To achieve further improvement in energy density and power capability, Li-ion hybrid electrochemical capacitors (Li-HEC) are fabricated with Nb_2O_5/graphene nanocomposite as anode and rice husk-derived activated porous carbon as cathode, in non-aqueous electrolyte. The Li-HEC showed enhanced electrochemical performances with high energy density of 30 $WhKg^{-1}$, at specific power density of 500 WKg^{-1}. The Nb_2O_5/graphene nanocomposites show promising results and hence have great potential for application in efficient electrochemical energy storage devices.

1. Introduction

With the ever-increasing demand for energy storage, lithium ion battery and supercapacitors has been the attractive technologies that has revolutionized the portable electronic industry and high power device applications.[1, 2] It is interesting to note that the materials design of these electrochemical energy storage device would vary with different energy domains of applications largely Li-ion battery and supercapacitors.[2-4] Recently, with the advancements in micro/nanoelectronics, lots of efforts are being undertaken to develop lighter, smaller and powerful rechargeable batteries with operating voltage in the range 1.9–2.5 V, thanks to the microfabrication technology enabled reduction of operating voltage of these devices to ~ 2V or less.[5] Electrode materials with high electrical conductivity for fast electron transport, and large surface area with short diffusion path for fast lithium ion diffusion, are essential to meet the high power requirements of these power sources.[6, 7]

Under such voltage and power requirements, several materials have been studied as alternative electrodes for rechargeable lithium batteries, among which, second row transition metal oxides (MoO_3, Nb_2O_5)[8, 9] have been explored recently due to their excellent structural stability and higher valence state of Nb_2O_5 and MoO_3. These metals contain two or more electrons available for the lithium insertion/extraction, thus offering the possibility of attaining an improved specific capacity over the existing ones. Among them, Nb_2O_5 with a theoretical capacity of 201 $mAhg^{-1}$ with 2 lithium insertion into $Li_xNb_2O_5$, is very promising as cathode material for 2V rechargeable lithium batteries, especially for microelectronic device applications. Recently, lithiated Nb_2O_5 electrode materials were explored for understanding its structural and electrochemical properties for energy storage applications.[10] Nb_2O_5 exists in several crystal structures depending on synthesis temperature that includes pseudo-hexagonal (500°C), orthorhombic (600-800°C), metastable tetragonal (1000°C), and monoclinic (1100°C). Kodama et. al.,[2] have investigated the variation of electrochemical performance with the change in crystal structure of Nb_2O_5 and found that the orthorhombic Nb_2O_5 (T-Nb_2O_5) is the most favorable phase shown to have excellent electrochemical performance due to enhanced reversible capacity (no capacity fading) and excellent reversible structural change during charge/discharge process, although it has lower capacity than the monoclinic.[11] The presence of 3-dimensional structure in orthorhombic Nb_2O_5 facilitates insertion of large amount of Li ions into the interstitial sites, and retains the original crystal lattice upon de-intercalation with very small change in the unit cell volume. Moreover, the chemical diffusion coefficient of Li^+ ions in T-Nb_2O_5 is about 10^{-10} cm^2s^{-1} which is same as the graphite electrode, and these factors favour orthorhombic phase as a potential cathode for lithium battery.[12, 13] Further, charge carrier conduction from the electrode to the current collectors and electrolyte diffusion during lithium intercalation are critical factors for improving the working efficiency of electrochemical systems like lithium batteries and supercapacitors.[14] Though there has been recent studies on high pseudocapacitive energy storage in Li intercalated Nb_2O_5 nanocrystals,[15, 16] particle-particle electronic

[a] School of Physics, Indian Institute of Science Education and Research Thiruvananthapuram, CET Campus, Sreekaryam, Thiruvananthapuram, Kerala, INDIA E-mail: shaiju@iisertvm.ac.in Phone: 04712599417
Electronic Supplementary Information (ESI) available: See DOI: 10.1039/x0xx00000x
[b] Present address: Postdoctoral Research Associate, School of Materials Science and Engineering, Chonnam National University, Gwangju 500-757, Republic of Korea.
* Email: shaiju@iisertvm.ac.in. Fax: +91-471-2597427. Tel: +91-471-2599417

conduction pathways is very critical in achieving high power capability at the nanoscale. However, the fabrication of nanostructures involves serious issues of heavy aggregation of nanocrystals due to van-der-Waal's forces between the particles that limits the special properties and causes structural instability thereby reducing its applicability. To prevent aggregation, nanocomposites consisting of nanoparticles decorated within a conducting substrate may be exploited, which preserves the unique properties of nanoparticles with high surface area along with imparting high electrical conductivity.[17] One such substrate is Graphene that offers large anchoring sites for the inorganic nanostructures due to its large surface area of ~2630 m^2g^{-1} and high 2-dimensional environment for fast electron transport through the conducting zero bandgap graphene layers.[18-23]

Here, we report a high conducting Nb_2O_5 decorated graphene nanocomposite with low graphene content (4.5 wt%), synthesized *via* hydrothermal approach, as an advanced electrode material for electrochemical energy storage. The synthesized Nb_2O_5 nanoparticles of size ~50 nm, decorates homogeneously throughout the graphene sheets. Electrochemical characterizations including cyclic voltammetry, galvanostatic charge/discharge and electrochemical impedance spectroscopy have been carried out to study the electrochemical performance of these electrodes as anodes for Li-ion battery. Further, a Li-ion hybrid electrochemical capacitor (Li-HEC) was fabricated with Nb_2O_5/graphene nanocomposite as anode and rice husk-derived carbon activated with H_3PO_4 (RHDPC-H_3PO_4) and KOH (RHDPC-KOH) as cathode, in non-aqueous electrolyte.

2. Experimental Methods

2.1 Synthesis of pristine Nb_2O_5 and Nb_2O_5 anchored graphene nanocomposite

Hydrothermal method was employed to synthesize pristine Nb_2O_5 and graphene anchored Nb_2O_5 nanocomposite. In a typical reaction, Niobium chloride (0.9 g) was dissolved in 15 ml of ethanol under ultrasonication for 0.5 h. Graphene oxide (0.045 g) was dispersed in 15 ml of deionized water to get graphene oxide (GO) dispersion. GO dispersion was added into the niobium chloride solution and ultrasonicated for 2 h to get a pale green colored sol. The sol was transferred to a 50 ml Teflon-lined autoclave and heated at 160 °C for 12 h. The resulting black precipitate was filtered and washed repeatedly with ethanol and deionized water and dried at 60 °C overnight in air oven. The synthesized Nb_2O_5/GO nanocomposite was then annealed at 700 °C in argon atmosphere to form Nb_2O_5 anchored graphene nanocomposite. GO was synthesized by following the procedure reported elsewhere.[24] The pristine Nb_2O_5 nanoparticles were synthesized by following the above mentioned procedure without graphene oxide.

2.2 Materials characterization

All the synthesized samples are characterized using the following instruments. Crystal structure was analyzed using Emperean, PANalytical XRD instrument with Cu Kα radiation, morphology analysis using Nova NanoSEM 450 FESEM, voltage range of 10-30 KV and JEOL JEM 2100, (200 kV) with LaB6 electron gun. Graphene content in the nanocomposite was determined using SDT Q600 Thermogravimetric analyzer and Raman analysis was carried out using LaBRAM HR Raman spectrometer, Horiba Jobin Yvon with 633 nm He-Ne Laser source. Surface area measurements were studied using N2 adsorption-desorption isotherms measured at 77 K up to a maximum relative pressure of 1 bar, with the Micromeritics 3-Flex surface characterization analyzer. Electrical conductivity measurements were studied by van der paw method.

2.3 Electrochemical Measurements

The working electrodes for lithium ion batteries were fabricated by mixing 80 wt% active material (pristine Nb_2O_5 and Nb_2O_5 anchored graphene nanocomposite), 10 wt% polyvinylidene fluoride binder and 10 wt% acetylene black, using 1-methyl-2-pyrrolidinone as dispersing solvent. The prepared slurries were coated on stainless steel foil and the electrodes were dried at 120 °C in vacuum overnight to remove the solvent. Electrochemical performance of Nb_2O_5 anchored graphene nanocomposite were studied *vs.* Li metal anode using CR2032 coin-type cell, glass microfiber filter paper as separator, and 1M $LiPF_6$ in a mixture of ethylene carbonate (EC) and dimethyl carbonate (DMC) (EC/DMC, 1:1 v/v) as the electrolyte. Electrochemical measurements such as cyclic voltammetry (CV) conducted at a scan rate of 0.05 mVs^{-1}, galvanostatic charge-discharge cycled between 1.0–3.0 V voltage window versus Li^+/Li and electrochemical impedance spectroscopy (EIS), were carried out using 16 channel VMP3 Biologic electrochemical workstation. The Li-HEC was fabricated with Nb_2O_5/graphene nanocomposite as negative electrode and rice husk derived porous carbon, activated using KOH (RHDPC-KOH) and H_3PO_4 (RHDPC-H_3PO_4), as positive electrodes. The electrode composition of 80:10:10 was maintained. Optimized mass loading ratio of 1:3 and 1:4 (anode:cathode) was used, respectively, with rice husk derived porous carbon activated with RHDPC-KOH and RHDPC-H_3PO_4.

3. Results and Discussion

Nb_2O_5/graphene nanocomposite was synthesized by anchoring crystalline Nb_2O_5 nanoparticles onto exfoliated graphene oxide (GO) in homogenous solution-phase and consequent conversion of amorphous Nb_2O_5/GO into Nb_2O_5/graphene nanocomposite by annealing at 700°C in the presence of argon atmosphere (Fig. 1). The mechanism for the synthesis of Nb_2O_5 decorated graphene is based on the attraction of the positively charged Niobium ions (Nb^{5+}) by the polarized bonds of the functional groups on GO and its subsequent oxidation to Nb_2O_5 followed by thermal reduction of GO into graphene under inert atmosphere. Thermally reduced graphene oxide has been demonstrated as an effective matrix for the adhesion of nanoparticles due to considerable content of oxide functional groups on the basal planes and edges of the 2-D graphene material.[17]

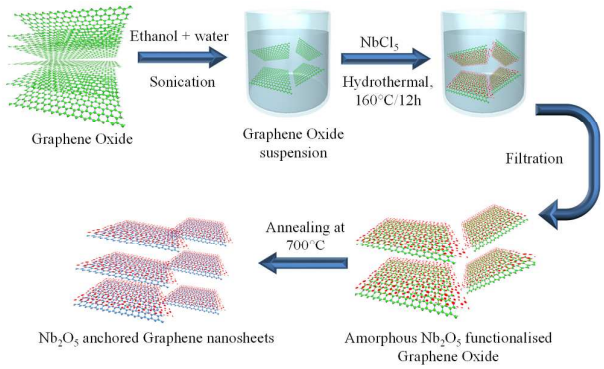

Fig. 1 Schematic illustration of the synthesis of Nb_2O_5 anchored graphene nanocomposite through hydrothermal method.

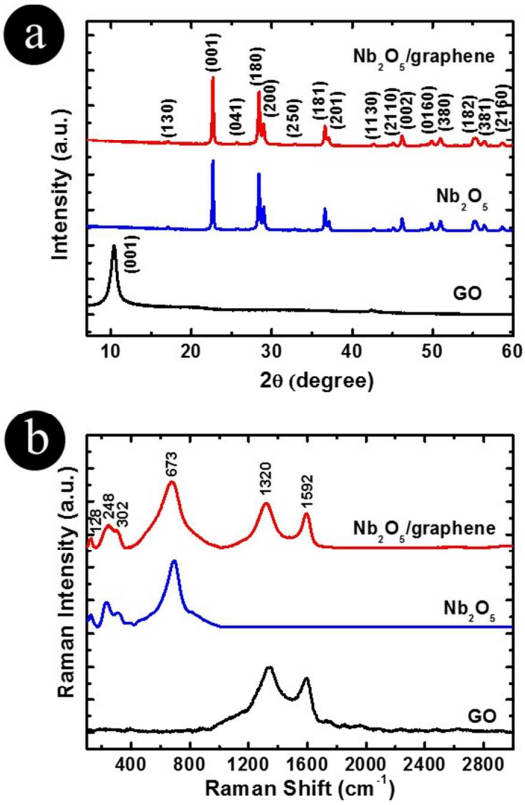

Fig. 2 (a) XRD and (b) Raman spectra of graphene oxide (GO), pristine Nb_2O_5 and Nb_2O_5/graphene nanocomposites.

A layered structure of orthorhombic Nb_2O_5 and Nb_2O_5/graphene nanocomposite was obtained with phase purity, without any impurity of other Nb_2O_5 polymorphs as evidenced from powder X-ray diffraction patterns, indexed with ICDD no. 30-0873 and space group: *Pbam* (Fig. 2a). Nb_2O_5 particles thus obtained has preferential orientation growth towards (001) plane, and small diffraction peak at ~26° for Nb_2O_5/graphene nanocomposite is attributed to the disordered graphene sheets which overlap with (041) plane of Nb_2O_5.[19] This low intense broad band also reveals the presence of highly disordered graphene sheets with no evidence of restacking of individual sheets, which is expected to be facilitated by the presence of surface anchored Nb_2O_5 nanoparticles. GO shows typical diffraction signature at ~10° which was not observed for the Nb_2O_5/graphene nanocomposite confirming the complete thermal reduction of graphene oxide into exfoliated graphene sheets. The weight percentage of the graphene in the Nb_2O_5/graphene nanocomposite based on the thermogravimetric analysis was estimated to be 4.5 wt% (Fig. S1, Supporting information).

Raman spectrum of the GO, Nb_2O_5 and Nb_2O_5/graphene nanocomposite are depicted in Fig. 2b. A broad Raman band ~ 420-990 cm^{-1} centered at ~680 cm^{-1} for pristine Nb_2O_5 and graphene nanocomposite are attributed to the symmetric and asymmetric stretching modes of Nb_2O_5. Other peaks in the lower Raman shift region (<300 cm^{-1}) match with the earlier reports.[25, 26] GO and Nb_2O_5/graphene nanocomposites show distinctive D and G Raman bands at ~1320 and ~1592 cm^{-1} respectively. D/G band ratio above unity illustrates the defective nature of graphene sheets caused by the surface decorated Nb_2O_5 nanoparticles. Scanning electron microscopy images of pristine Nb_2O_5 and Nb_2O_5/graphene nanocomposites are shown in Fig. 3a,b respectively. The Nb_2O_5 nanoparticles are ~50 nm sized polyhedral particles (Fig. 3a), while the graphene sheets are uniformly decorated with a dense network of Nb_2O_5 nanoparticles in Nb_2O_5/graphene nanocomposites (Fig. 3b). High-resolution TEM images of Nb_2O_5 and graphene nanocomposite are shown in Fig. 3c,d respectively. It is to be noted that Nb_2O_5 nanoparticles seem to agglomerate forming clusters (~100 nm diameter), as evidenced in the SEM (Fig. 3a and Fig. S2a, Supporting information) and TEM images (Fig. 3c). However, interestingly, the SEM images (Fig. 3b and Fig. S2b, Supporting information) and TEM images of nanocomposite (Fig. 3d and Fig. S2c, Supporting information) show smaller Nb_2O_5 nanoparticles (~25 nm) anchored on to the graphene sheets, with negligible agglomeration. Formation of such nanocomposite has resulted in dense packing of homogeneously distributed Nb_2O_5 nanoparticles on few layer-graphene sheets, which further lead to much improved electrochemical performance, as explained in succeeding sections. Nb_2O_5 nanoparticles exhibit high crystallinity with lattice spacing of 0.39 nm (inset of Fig. 3d), attributed to the interspacing of (001) plane, which is consistent with the results obtained from XRD analysis (Fig. 2a). Electrical conductivity measurements carried out using van der Pauw method on the Nb_2O_5/graphene nanocomposite material showed excellent conductivity of 0.45 S m^{-1}, compared to that of ~6 x 10^{-7} S m^{-1}, measured for prisitine Nb_2O_5. Large enhancement in the BET surface area was also exhibited by Nb_2O_5/graphene nanocomposite (112 m^2 g^{-1}) compared to measured BET surface area of 22 m^2 g^{-1} for pristine Nb_2O_5 (Fig. S3a, Supporting information). Metal oxide/graphene nanocomposites with different architectures, namely encapsulated, sandwiched, layer-by-layer assembled and anchored have recently been explored as advanced electrode materials for energy applications. These nanocomposites, as reported in literature, show noteworthy results in enhancing the electrochemical properties due to their synergistic effect compared to the respective individual components, but basically with very high graphene content (>25 wt%), which includes the

electrochemical lithium intercalation into graphene interlayers.[27-29]

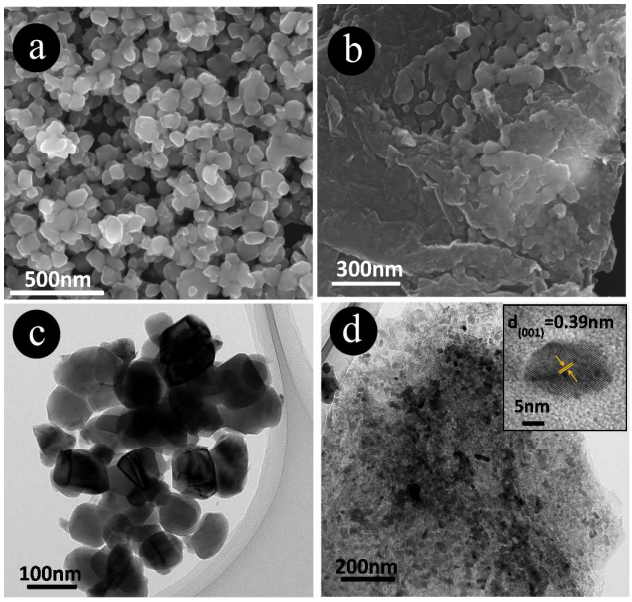

Fig. 3 SEM images of (a) Nb_2O_5 nanocrystals (b) Nb_2O_5/graphene nanocomposite and TEM images of (c) pristine Nb_2O_5 nanocrystals and (d) Nb_2O_5/graphene nanocomposite. Inset of figure 4d shows the high resolution TEM image of Nb_2O_5 nanocrystal.

In the present work, we explore the electrochemical performance of Nb_2O_5/graphene nanocomposites as electrode for high power lithium battery through the increased surface area of active Nb_2O_5 nanoparticle which decorates onto the conducting graphene layers which would enhance the overall battery performance.[30] Here, 4.5 wt% of graphene in the composite electrode, acts as dispersing matrix for anchoring the Nb_2O_5 nanoparticle and, does not involve in the electrochemical lithiation/delithiation process.

The electrochemical performance of pristine Nb_2O_5 and Nb_2O_5/graphene nanocomposites were investigated by carrying out half-cell measurements *vs.* Li metal anode, in a coin cell assembly. The galvanostatic cycling curves and cyclic voltammograms (CV) of the pristine Nb_2O_5 are shown in Fig. 4a and b, respectively. Both these studies are carried out in the potential window of 1.0 - 3.0 V *vs.* Li/Li^+, at 25 °C. CV measurements were performed at a scan rate of 0.05 mVs^{-1}. The electrochemical intercalation-deintercalation reaction of lithium with Nb_2O_5 occurs as follows,[16]

$$Nb_2O_5 + xLi^+ + xe^- \rightarrow Li_xNb_2O_5 \qquad (1)$$

with a maximum lithium uptake of $x = 2$. The voltage profile shows a sloppy curve which is characteristic of orthorhombic Nb_2O_5 (Fig. 4a) that agrees with the reported literature.[9] The discharge voltage decreases with increasing capacity, which is more prominent in the first discharge cycle. The first discharge curve with line profile indicates the formation of lithiated niobium oxide ($Li_xNb_2O_5$) during lithium intercalation, where x value varies between 0 and 2. The CV of pristine Nb_2O_5 (Fig.

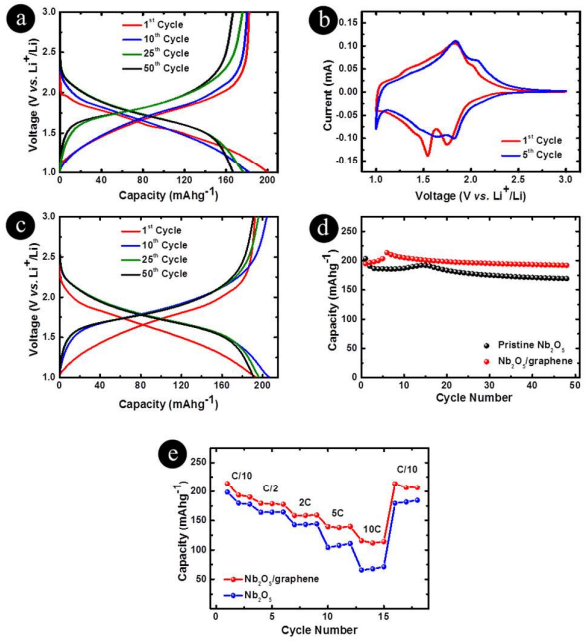

Fig. 4 (a) Voltage profile and (b) Cyclic voltammogram of Pristine Nb_2O_5 nanocrystals, (c) Voltage profile of Nb_2O_5/graphene hybrid nanocomposite, (d) Capacity vs. cycle no of pristine Nb_2O_5 and Nb_2O_5/graphene nanocomposite at C/10 rate and (e) rate capability measurements showing cycling at different rates for pristine Nb_2O_5 and Nb_2O_5/graphene nanocomposite electrodes.

4b) showed cathodic peaks at 1.54 V and 1.74 V and anodic peaks at 1.84 V and 2.0 V in the first cycle, which indicates Li ion intercalation/deintercalation process. This reveal that the lithium ion intercalation process in orthorhombic Nb_2O_5 could be a complex two-step process.[9] With the increase in number of cycles, broadening and shifting of cathodic peaks occur at 1.64 V and 1.83 V, whereas the anodic peaks appear to be stationary.[9] The shift in the cathodic peaks could be due to the polarization of the electrode in the first cycle.[31] Moreover, first few cycles are the formation cycles that form good electrical contact between active material, binder, conducting carbon and current collector.

Electrochemical characteristics of Nb_2O_5 decorated graphene nanocomposite electrode *vs.* Li, was studied under same experimental condition. It is clear from the voltage profiles that the capacity of the nanocomposite has increased slightly despite the fact that the graphene in the nanocomposite does not intercalate with lithium at these potentials (Fig. 4c). The lithium insertion potential in pure graphene layers were reported to occur close to 0.1 V *vs.* Li/Li^+ reference electrode.[32] The increase in capacity of graphene composite may be attributed to the improved surface area of the composite electrode, as evidenced from the BET surface area measurements, (Fig. S3a, Supporting information) leading to enhanced electrochemical activity. The decoration of Nb_2O_5 nanoparticles in the graphene sheets has resulted in the improved conductivity of the whole electrode material which is also confirmed from the four probe

conductivity measurements. With improvement in conductivity of the material, the kinetic constraint will be greatly reduced resulting in better cycling performances.

The cycling performance of pristine Nb_2O_5 nanocrystals and Nb_2O_5/graphene nanocomposite are studied at a cycling rate of C/10 (1C = 200 mA g^{-1}) (Fig. 4d). Much higher capacity, closer to theoretical value, has been obtained for the nanocomposite electrode, when cycled at C/10 rate. The first discharge capacity of pristine Nb_2O_5 and Nb_2O_5/graphene nanocomposite electrodes were 204 and 195 $mAhg^{-1}$, respectively, at C/10 rate. A slight increase in the discharge capacity was observed in the initial cycles, which could be due to the nanosize effect of the electrode material, as reported earlier.[33] The reversible discharge capacity of Nb_2O_5/graphene nanocomposite was higher than the pristine Nb_2O_5, after 50 cycles at C/10 rate, with 192 and 166 $mAhg^{-1}$, respectively. These capacity values correspond to ~2.0 and 1.7 moles of lithium per mole of T-Nb_2O_5 (x = 2.0 and 1.7 in $Li_xNb_2O_5$) inserted for Nb_2O_5/graphene nanocomposite and pristine Nb_2O_5, respectively, during discharge cycle. High cyclic stability of the nanocomposite electrode at higher current rates has been demonstrated. The nanocomposite electrode cycled at 1C rate clearly showed improved performance with ~160 $mAhg^{-1}$ upto 50 cycles, compared to ~115 $mAhg^{-1}$ for pristine Nb_2O_5 nanoparticles (Fig. S4, Supporting information). The rate capability of these two electrodes was investigated by galvanostatic cycling measurements under different C rates from C/10 to 10 C (Fig. 4e). The specific capacity of graphene composite at high rates of 10 C showed 115 $mAhg^{-1}$ which is ~55% capacity retention compared with C/10 rate. Discharge capacity of 70 $mAhg^{-1}$ was observed for pristine sample at 10 C rate, with capacity retention of 35% with respect to capacity under C/10 rate. High capacity retention of graphene composite with highly dispersed T-Nb_2O_5 nanoparticles, also results from the presence of 3-dimensional Wadsley-Roth phase in the flexible Nb_2O_5 crystal structure.[34] In pristine Nb_2O_5, large aggregation of the nanoparticles decreases the real surface area and the availability of vacant interstitial sites of the Nb_2O_5 nanoparticles causing low capacity retention at high C rate.

X-ray photoelectron spectroscopy was used to investigate the valence state of the elements in the Nb_2O_5/graphene nanocomposite which reveals the presence of Nb^{5+} species in the electrode (Fig. S5, Supporting information). Stability and the morphological changes of pristine Nb_2O_5 and graphene composite electrodes upon electrochemical cycling were investigated by SEM of cycled electrode (Fig. S6, Supporting information), which clearly show that Nb_2O_5 nanoparticles had no morphological change after lithiation/deliathation cycles. This results from the superior structural stability and near zero volume expansion of Nb_2O_5 nanoparticles.

The superior electrochemical performance of Nb_2O_5/graphene nanocomposite may be attributed to the following reasons. (a) The presence of flexible, thin graphene sheets that acts as support for the anchoring of Nb_2O_5 nanoparticles. The graphene sheets provide an effective buffering layer for Nb_2O_5 particles apart from its own structural voids during lithium intercalation and prevent the aggregation of Nb_2O_5 nanoparticles upon cycling thus realizing high reversible capacity, capacity retention and power capability.[19, 35] (b) Graphene sheets provide high electrical conductivity and delivers conductive pathways between individual Nb_2O_5 nanoparticles which decrease internal resistance leading to higher reversible capacity.[36, 37] (c) Kinetics of lithium transport depends on the path length and vacant active sites on the surface of electrode.[38] Hence the graphene nanocomposite provides large electrode/electrolyte interfacial area, shorter path length for Li^+ transport maintaining the structural integrity of the self-supported nanoarchitectural electrode. (d) Anchored Nb_2O_5 nanoparticles efficiently prevents the restacking of graphene sheets maintaining high surface area of graphene sheets.[19]

The formation of graphene composite with low amount of graphene content (4.5 wt%) is expected to increase the overall conductivity of the electrode, which was confirmed by electrochemical impedance spectroscopic analysis. The Nyquist plots of pristine and graphene composite electrodes before and after cycling are shown in Fig. 5a. The charge transfer resistance (R_2) of the pristine Nb_2O_5 nanoparticles and Nb_2O_5/graphene nanocomposite before cycling was found to be 135.3 and 61.2 Ω respectively. When EIS analysis was done on these cells after carrying out galvanostatic charge/discharge for 50 cycles, R_2 for pristine Nb_2O_5 nanoparticles and Nb_2O_5/graphene nanocomposite increased to 150.9 Ω and 67.5 Ω respectively. This shows that the graphene scaffoldings provide good electronic conductivity for the niobate nanoparticles resulting in the reduction of the overall resistance of the nanocomposite material. A detailed EIS analysis using equivalent circuit has been carried out (Fig. S7, Table S1, supporting information). The power capability of the electrode depends greatly on its electronic conductivity and the availability of real surface area of active material for the lithiation/delithiation process which would also enhances the kinetics of lithium insertion. To further investigate the rate capability of the composite electrode, typical 'signature curve' studies have been carried out on the two electrodes (Fig. 5b). For this, both pristine Nb_2O_5 nanoparticles and the Nb_2O_5/graphene nanocomposites were discharged at a very slow rate of C/20 and continuous charging cycles were carried out from 16C to C/32 by giving a rest time of 5 min in between to obtain the signature curve data. However to investigate the role of graphene and its conductivity (similar to conductive carbon additive) on rate capability of Nb_2O_5 graphene composite at high C rates, signature curve was obtained for the pristine Nb_2O_5 electrode (depicted as Nb_2O_5 - 1) with excess additive carbon black (Nb_2O_5 - 2) and excess graphene content (Nb_2O_5 - 3) apart from the defined cell fabrication composition of 80 wt% - active material, 10 wt% - carbon black and 10 wt% pvdf (Nb_2O_5 - 1). While pristine Nb_2O_5 (Nb_2O_5 - 1) showed only 30 % capacity retention at high current rate of 16C, Nb_2O_5 – 2 and Nb_2O_5 – 3 with 5 wt% excess carbon black and 5 wt% excess graphene (thermally reduced graphene oxide) respectively, delivered capacity retention of 42%.

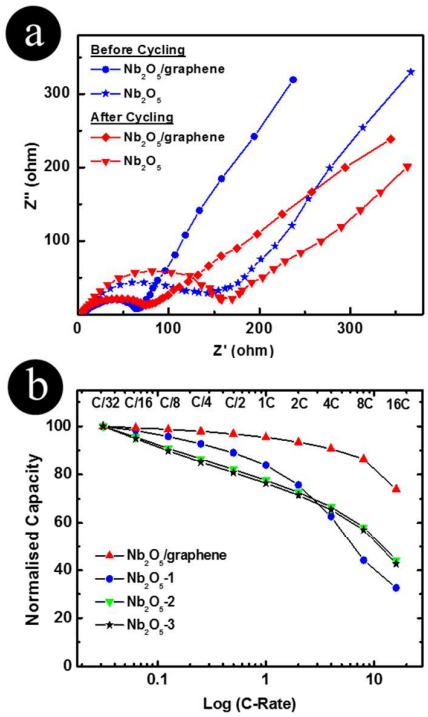

Fig. 5 (a) Electrochemical impedance spectroscopy plots for Nb_2O_5 and Nb_2O_5/graphene nanocomposite electrodes, (b) 'Signature' curve plots of pristine Nb_2O_5 (Nb_2O_5-1) and Nb_2O_5/graphene hybrid with different compositions of conductive carbon in the Nb_2O_5 electrode. The materials under investigation are **Nb_2O_5/graphene nanocomposite:** Nb_2O_5/Graphene = 80 wt%, where the graphene content in the composite is ~5 wt% ; Acetylene black = 10 wt%; and PvdF = 10 wt%, **Nb_2O_5 – 1 (Pristine Nb_2O_5):** Nb_2O_5 = 80 wt%; Acetylene black = 10 wt%; and PvdF = 10 wt%, **Nb_2O_5 – 2:** Nb_2O_5 = 75 wt%; Acetylene black = 15 wt%; and PvdF = 10 wt%, **Nb_2O_5 – 3:** Nb_2O_5 = 75 wt%; Acetylene black = 10 wt%; graphene = 5 wt% and PvdF = 10 wt%.

However, Nb_2O_5 decorated graphene composite which possess 4.5 wt% of thermally reduced graphene oxide showed enormous capacity retention of 80% at 16 C rate. This clearly demonstrate the role of graphene in the composite as a conducting substrate, which in addition, act as anchoring sites for well dispersed electroactive Nb_2O_5 nanoparticles, thus realizing high surface area for the lithiation/delithiation process and thereby improving the kinetics of lithium intercalation/de-intercalation in the electrode.

The good insertion nature of Nb_2O_5/graphene nanocomposite makes it a suitable electrode in a Li-ion hybrid electrochemical capacitor (Li-HEC). Li-HEC combines both the battery and supercapacitor electrodes, such that it can achieve higher energy density than EDLC and higher power density than Li-ion batteries, with high cycling stability.[39-41] It contains a faradaic anodic part where Li intercalation takes place and a non-faradaic cathodic part where anionic adsorption occurs.[42, 43] Here, a Li-HEC was fabricated with Nb_2O_5/graphene nanocomposite as anode and rice husk-derived activated porous carbon (RHDPC) as cathode in a non-aqueous electrolyte (1M $LiPF_6$ in 1:1 v/v EC-DMC). The electrochemical performance was studied between 1.0 – 3.0 V at various current densities. At the cathode side, two types of RHDPCs [44] – one, activated with KOH (RHDPC-KOH) and the other with H_3PO_4 (RHDPC-H_3PO_4), with varying BET surface area were used. RHDPC-KOH exhibits high surface area of 1809 m^2g^{-1}, while RHDPC-H_3PO_4 shows surface area of 1256 m^2g^{-1} (Fig. S3b, Supporting information). The electrode mass loading plays a crucial role in the fabrication of hybrid device.[45] The mass ratio has been calculated from individual measurements of each electrodes with respect to the Li-reference electrode (Fig. S8, Supporting information). Electrochemical voltage profiles of the Nb_2O_5-graphene / RHDPC-KOH and the Nb_2O_5-graphene / RHDPC-H_3PO_4 devices were obtained in the voltage range between 1 and 3 V at different current densities (based on the total active mass) and the results are illustrated in Fig. 6 a,b respectively. The remarkable features of the discharge curves in Li-HEC comprises of three important regions, such as, IR drop due to the ohmic resistance offered by active material, the monotonous curve region due to Li-extraction from the lattice of Nb_2O_5-graphene and simultaneous de-sorption of PF_6^- ions from the active sites of porous carbon and the sudden drop.[46]

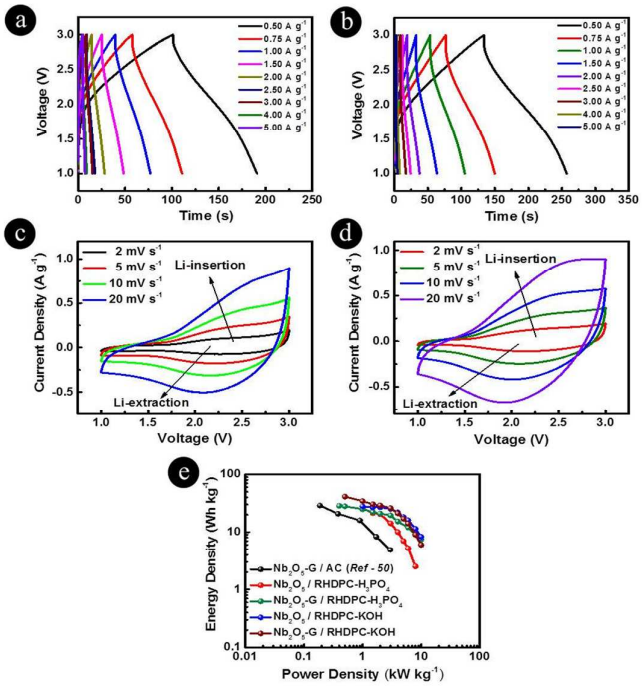

Fig. 6 Galvanostatic charge-discharge curves of Li-HEC with (a) Nb_2O_5-graphene / RHDPC- H_3PO_4 electrodes (b) Nb_2O_5-graphene / RHDPC – KOH electrodes, at different applied current densities. Cyclic Voltammograms of (c) Nb_2O_5-graphene / RHDPC- KOH electrodes (d) Nb_2O_5-graphene / RHDPC – H_3PO_4 electrodes; (e) Ragone plot of different Li-HEC configurations in comparison with the reported binder-free Nb_2O_5@graphene and activated carbon (Nb_2O_5-G/AC)[50].

The electrode delivered a specific capacity of 34 F g^{-1} at 0.5 A g^{-1}. Cyclic voltammetry (CV) performed for the device (Fig. 6 c,d) showed a drastic increase/decrease in current response at above/below 1.5 V which is attributed to the Li-insertion/extraction in to/from the Nb_2O_5 lattice. Fig. 6e shows the ragone plot, representing the energy density *vs.* power densities of two devices with different cathode materials namely, RHDPC-H_3PO_4 and RHDPC-KOH. Nb_2O_5-graphene/RHDPC-KOH device showed improved electrochemical performance with maximum energy density of 30 Wh kg^{-1} and power density of 10 kW kg^{-1} at current rate of 5 Ag^{-1}, compared to Nb_2O_5-graphene / RHDPC-H_3PO_4 device (Fig. 6e). This could be attributed to the enhanced surface area of RHDPC-KOH electrode, resulting in more activation sites for accomodating PF_6^- ions during electrochemical processes.[47-49] Li-HEC devices fabricated using pristine Nb_2O_5/RHDPC electrodes showed similar electrochemical behavior, as evidenced from their galvanostatic cycling profiles and cyclic voltammograms (Fig. S9, Supporting information). Graphene nanocomposite electrode exhibited better power and energy densities compared to the pristine Nb_2O_5/RHDPC electrodes and the results obtained here are better than the earlier reports on binder-free Nb_2O_5@graphene electrodes.[50] To further investigate the effect of graphene content on the electrochemical properties Nb_2O_5-graphene, Li-HEC devices are fabricated with RHDPC-KOH as cathode and Nb_2O_5-graphene composite with varying graphene content (NG-10% , NG-20% and NG-40%), as anode. The NG-10% , NG-20% and NG-40% contains ~ 4.5 wt%, ~ 7.5 wt% and ~ 14 wt% of graphene, respectively, as observed from the TG analysis (Fig. S10, Supporting information). From the ragone plot (Fig. S11, Supporting information), it is clear that NG-20% composite exhibits the best performance, which could be the optimum loading of graphene in terms of better dispersion. Thus the fabricated Nb_2O_5/graphene nanocomposite showed promising results as electrode material for high power eletrochemical energy storage devices.

4. Conclusions

Self-supported nanoarchitectural electrode with Nb_2O_5 decorated graphene was fabricated through simple strategy, and has been demonstrated as promising electrode for rechargeable lithium battery and Lithium ion hybrid capacitor. Excellent electrochemical performance of the graphene composite electrode was attributed to the uniform decoration of Nb_2O_5 nanoparticles over graphene sheets and the realization of high surface area for the lithation/delithiatition process to occur. Graphene nanocomposite with good mechanical flexibility, high surface area and improved structural integrity, enhances the kinetics of lithium intercalation due to short diffusion path for Li^+ transport, resulting in high power capabilities. Graphene composite with low graphene content (4.5 wt%) delivered specific capacity of 192 $mAhg^{-1}$ compared to 166 $mAhg^{-1}$ for pristine sample after 50 cycles at C/10. Signature curve studies clearly revealed high power capability of graphene composite with capacity retention of 80% compared to 30% for pristine electrode at very high current rate of 16 C. Li-ion hybrid electrochemical capacitor devices fabricated with Nb_2O_5-graphene as anode and RHDPC as cathode, showed excellent electrochemical performances. With such superior electrochemical characteristics, Nb_2O_5 anchored graphene nanocomposite could be an ideal electrode for high performance electrochemical energy storage devices.

Acknowledgements

The work has been partly supported by Department of Science & Technology (DST), Govt. of India, through DST Fast-track scheme for Young Scientists (No:SR/FTP/PS-081/2010), the Board of Research in Nuclear Sciences (BRNS), Department of Atomic Energy (DAE), Govt. of India, through a DAE Young Scientist Research Award (No. 2012/20/34/5/BRNS) and Department of Biotechnology (DBT), Govt. of India, under DBT's Twinning programme for the NE (No: BT/350/NE/TBP/2012).

Notes and references

1. J. M. Tarascon and M. Armand, *Nature*, 2001, **414**, 359-367.
2. P. Simon and Y. Gogotsi, *Nat Mater*, 2008, **7**, 845-854.
3. W. Zuo, C. Wang, Y. Li and J. Liu, *Sci. Rep.*, 2015, **5**.
4. L. Chen, Q. Zhang, H. Xu, X. Hou, L. Xuan, Y. Jiang and Y. Yuan, *J. Mater. Chem. A*, 2015, **3**, 1847-1852.
5. R. Kodama, Y. Terada, I. Nakai, S. Komaba and N. Kumagai, *J. Electrochem. Soc.*, 2006, **153**, A583-A588.
6. Z.-S. Wu, W. Ren, L. Xu, F. Li and H.-M. Cheng, *ACS Nano*, 2011, **5**, 5463-5471.
7. A. L. M. Reddy, S. R. Gowda, M. M. Shaijumon and P. M. Ajayan, *Adv. Mater.*, 2012, **24**, 5045-5064.
8. P. Meduri, E. Clark, J. H. Kim, E. Dayalan, G. U. Sumanasekera and M. K. Sunkara, *Nano Lett.*, 2012, **12**, 1784-1788.
9. A. L. Viet, M. V. Reddy, R. Jose, B. V. R. Chowdari and S. Ramakrishna, *J. Phys. Chem. C*, 2010, **114**, 664-671.
10. M. Catti and M. R. Ghaani, *Phys. Chem. Chem. Phys.*, 2014, **16**, 1385-1392.
11. G. Park, N. Gunawardhana, C. Lee, S.-M. Lee, Y.-S. Lee and M. Yoshio, *J. Power Sources*, 2013, **236**, 145-150.
12. N. Kumagai, I. Ishiyama and K. Tanno, *J. Power Sources*, 1987, **20**, 193-198.
13. P. Yu, B. N. Popov, J. A. Ritter and R. E. White, *J. Electrochem. Soc.*, 1999, **146**, 8-14.
14. H. Wen, Z. Liu, J. Wang, Q. Yang, Y. Li and J. Yu, *Appl. Surf. .*, 2011, **257**, 10084-10088.
15. V. Augustyn, J. Come, M. A. Lowe, J. W. Kim, P.-L. Taberna, S. H. Tolbert, H. D. Abruña, P. Simon and B. Dunn, *Nat. Mater.*, 2013, **12**, 518-522.
16. K. Brezesinski, J. Wang, J. Haetge, C. Reitz, S. O. Steinmueller, S. H. Tolbert, B. M. Smarsly, B. Dunn and T. Brezesinski, *J. Am. Chem. Soc.*, 2010, **132**, 6982-6990.
17. H. N. H. Lim, N. M. Chia, C. H. Harrison, I., *Advanced Topics in Crystal Growth* 2013.
18. Y. Zhu, S. Murali, W. Cai, X. Li, J. W. Suk, J. R. Potts and R. S. Ruoff, *Adv. Mater.*, 2010, **22**, 3906-3924.
19. Z.-S. Wu, W. Ren, L. Wen, L. Gao, J. Zhao, Z. Chen, G. Zhou, F. Li and H.-M. Cheng, *ACS Nano*, 2010, **4**, 3187-3194.
20. Z.-F. Li, H. Zhang, Q. Liu, L. Sun, L. Stanciu and J. Xie, *ACS Appl. Mater. Interfaces*, 2013, **5**, 2685-2691.
21. P. Avouris, *Nano Lett.*, 2010, **10**, 4285-4294.

22. H. Chang and H. Wu, *Adv. Mater.*, 2013, **23**, 1984-1997.
23. Y. Sun, X. Hu, W. Luo, F. Xia and Y. Huang, *Adv. Funct. Mater.*, 2013, **23**, 2436-2444.
24. D. C. Marcano, D. V. Kosynkin, J. M. Berlin, A. Sinitskii, Z. Sun, A. Slesarev, L. B. Alemany, W. Lu and J. M. Tour, *ACS Nano*, 2010, **4**, 4806-4814.
25. B. X. Huang, K. Wang, J. S. Church and Y.-S. Li, *Electrochim. Acta*, 1999, **44**, 2571-2577.
26. S. Xie, E. Iglesia and A. T. Bell, *J. Phys. Chem. Soc.B*, 2001, 105, 5144-5152.
27. J. Lin, A.-R. O. Raji, K. Nan, Z. Peng, Z. Yan, E. L. G. Samuel, D. Natelson and J. M. Tour, *Adv. Funct. Mater.*, 2014, **24**, 2044-2048.
28. Q. Guo, Z. Zheng, H. Gao, J. Ma and X. Qin, *J. Power Sources*, 2013, **240**, 149-154.
29. J. Qin, C. He, N. Zhao, Z. Wang, C. Shi, E.-Z. Liu and J. Li, *ACS Nano*, 2014, **8**, 1728-1738.
30. D. Wang, D. Choi, J. Li, Z. Yang, Z. Nie, R. Kou, D. Hu, C. Wang, L. V. Saraf, J. Zhang, I. A. Aksay and J. Liu, *ACS Nano*, 2009, **3**, 907-914.
31. M. M. Rahman, R. A. Rani, A. Z. Sadek, A. S. Zoolfakar, M. R. Field, T. Ramireddy, K. Kalantar-zadeh and Y. Chen, *J. Mater. Chem. A*, 2013, **1**, 11019-11025.
32. A. Kumar, A. L. M. Reddy, A. Mukherjee, M. Dubey, X. Zhan, N. Singh, L. Ci, W. E. Billups, J. Nagurny, G. Mital and P. M. Ajayan, *ACS Nano*, 2011, **5**, 4345-4349.
33. M. Sasidharan, N. Gunawardhana, M. Yoshio and K. Nakashima, *Mater. Res. Bull.*, 2012, **47**, 2161-2164.
34. R. J. Cava, D. W. Murphy and S. M. Zahurak, *J. Electrochem. Soc.*, 1983, **130**, 2345-2351.
35. S.-M. Paek, E. Yoo and I. Honma, *Nano Lett.*, 2009, 9, 72-75.
36. P. V. Kamat, *J. Phys. Chem. Soc.*, 2010, **1**, 520-527.
37. Z.-S. Wu, W. Ren, L. Gao, B. Liu, C. Jiang and H.-M. Cheng, *Carbon*, 2009, **47**, 493-499.
38. C. Jiang, E. Hosono and H. Zhou, *Nano Today*, 2006, **1**, 28-33.
39. G. G. Amatucci, F. Badway, A. Du Pasquier and T. Zheng, *J. Electrochem. Soc.*, 2001, **148**, A930-A939.
40. W. G. Pell and B. E. Conway, *J. Power Sources*, 2004, **136**, 334-345.
41. K. Naoi, S. Ishimoto, J.-i. Miyamoto and W. Naoi, *Energy Environ. Sci.*, 2012, **5**, 9363-9373.
42. V. Aravindan, J. Gnanaraj, Y.-S. Lee and S. Madhavi, *Chem. Rev.*, 2014, **114**, 11619-11635.
43. J. Come, V. Augustyn, J. W. Kim, P. Rozier, P.-L. Taberna, P. Gogotsi, J. W. Long, B. Dunn and P. Simon, *J. Electrochem. Soc.*, 2014, **161**, A718-A725.
44. A. Ganesan, R. Mukherjee, J. Raj and M. Shaijumon, *J. Porous Mater.*, 2014, **21**, 839-847.
45. S. Dsoke, B. Fuchs, E. Gucciardi and M. Wohlfahrt-Mehrens, *J. Power Sources*, 2015, **282**, 385-393.
46. D. Puthusseri, V. Aravindan, S. Madhavi and S. Ogale, *Electrochim. Acta* 2014, **130**, 766-770.
47. A. Banerjee, K. K. Upadhyay, D. Puthusseri, V. Aravindan, S. Madhavi and S. Ogale, *Nanoscale*, 2014, **6**, 4387-4394.
48. V. Aravindan, D. Mhamane, W. C. Ling, S. Ogale and S. Madhavi, *ChemSusChem*, 2013, **6**, 2240-2244.
49. R. Gokhale, V. Aravindan, P. Yadav, S. Jain, D. Phase, S. Madhavi and S. Ogale, *Carbon*, 2014, **80**, 462-471.
50. L. P. Wang, L. Yu, R. Satish, J. Zhu, Q. Yan, M. Srinivasan and Z. Xu, *RSC Adv.*,, 2014, **4**, 37389-37394.

Graphical Abstract